ChemComm

COMMUNICATION

Cite this: *Chem. Commun.*, 2022, **58**, 10166

Received 21st April 2022,
Accepted 11th August 2022

DOI: 10.1039/d2cc02249d

rsc.li/chemcomm

Highly sensitive acetylcholine biosensing *via* chemical amplification of enzymatic processes in nanochannels†

Yamili Toum Terrones, [a] Gregorio Laucirica, [a] Vanina M. Cayón,[ab] Gonzalo E. Fenoy, [a] M. Lorena Cortez, [a] María Eugenia Toimil-Molares,[b] Christina Trautmann,[bc] Waldemar A. Mamisollé [a] and Omar Azzaroni *[a]

Acetylcholinesterase-modified nanochannels are proposed as reliable and reproducible nanofluidic sensors for highly sensitive detection of acetylcholine. The operation mechanism relies on the use of weak polyelectrolytes as "chemical amplifiers" that adjust/reconfigure the nanochannel surface charge in the presence of local pH changes induced by the enzymatic reaction. Experimental results show that the presence of acetylcholine can be transduced into measurable ionic signals with a low limit of detection.

In a recent report, the World Health Organization stated that neurological disorders such as epilepsy, Parkinson's disease or Alzheimer's disease are affecting nearly 1 in 100 of the world's inhabitants.[1] Neurodegenerative diseases cause progressive loss of cognitive and/or motor function and, as life expectancy rises, they imply major challenges for societies with rapidly aging populations.[2] As a result, monitoring neurotransmitters is becoming increasingly relevant in clinical environments. Acetylcholine (Ach) is a neurotransmitter that plays a key role in the communication between neurons in the spinal cord and nerve skeletal junctions in vertebrates.[3,4] Since an abnormal concentration of Ach has proven to be related to neurodegenerative diseases, novel strategies for highly sensitive and specific Ach (bio)sensing are always in great demand.[5] The physiological concentrations of Ach are in the nanomolar range and its detection and/or quantification are currently being achieved using expensive and time-consuming analytical techniques (such as liquid chromatography and capillary electrophoresis).[6–8] In this context, nanofluidic devices such as solid-state nanochannels (SSNs) have emerged as a promising sensing technology for quantitative neurotransmitter detection.[9] In the last few years, these devices have been proven to show rapid and sensitive detection of ions, small molecules, and biological macromolecules through the combination of versatile surface modification strategies with reliable nanofabrication techniques.[10] In this context, the integration of enzymatic functions into SSNs has enabled the development of novel nanofluidic elements with tailored sensory functions.[9,11] Inspired by these advances, in this work we show the construction of Ach enzymatic biosensors with remarkable sensitivity by immobilizing acetylcholinesterase (AchE) on polyamine-modified bullet-shaped single nanochannels *via* electrostatic self-assembly. We demonstrate that local pH changes caused by the confined enzyme-catalyzed hydrolysis of Ach affect the protonation degree of the nanochannel surface, constituting the signal transduction mechanism of the biosensor that allows the detection of the neurotransmitter in a steady-state configuration. In this configuration, the polyamine plays a key role as a "reactive signal amplifier" as it enhances the variations in the nanochannel surface charge as a result of the pH-shifting enzymatic process. The nanofluidic sensing device shows a highly reversible iontronic response towards Ach with appropriate selectivity in the presence of other analytes such as dopamine, serotonin, L-cysteine, ascorbic acid and, glucose.

Initially, the ion-track etching technique was employed to fabricate bullet-shaped single nanochannels in PET membranes.[12] To this end, the foil was irradiated with swift heavy ions and the resulting ion track was selectively dissolved in a highly basic aqueous solution (for the etching procedure, see the ESI,† file) to obtain a bullet-shaped nanochannel with a base diameter of 600 ± 28 nm and a tip diameter of 85 ± 7 nm (Fig. S1, ESI†).[13] The controlled PET hydrolysis exposed carboxylic groups at the channel surface. These groups endow the surface with a negative charge at pH > 4,[14] where the positively charged polyethylenimine (PEI) can be immobilized by immersing the membrane in a PEI aqueous solution (Fig. 1a), turning the surface charge positive.[15] After that, electrostatic immobilization was chosen for AchE anchoring to the PET/PEI SSN surface since, in contrast to covalent binding strategies, it allows preservation of the folding and the functionality

[a] *Instituto de Investigaciones Fisicoquímicas Teóricas y Aplicadas (INIFTA), Departamento de Química, Facultad de Ciencias Exactas, Universidad Nacional de La Plata, CONICET – CC 16 Suc. 4, 1900 La Plata, Argentina. E-mail: omarazzaroni@quimica.unlp.edu.ar*

[b] *GSI Helmholtzzentrum für Schwerionenforschung, 64291 Darmstadt, Germany*

[c] *Technische Universität Darmstadt, Materialwissenschaft, 64287 Darmstadt, Germany*

† Electronic supplementary information (ESI) available. See DOI: https://doi.org/10.1039/d2cc02249d

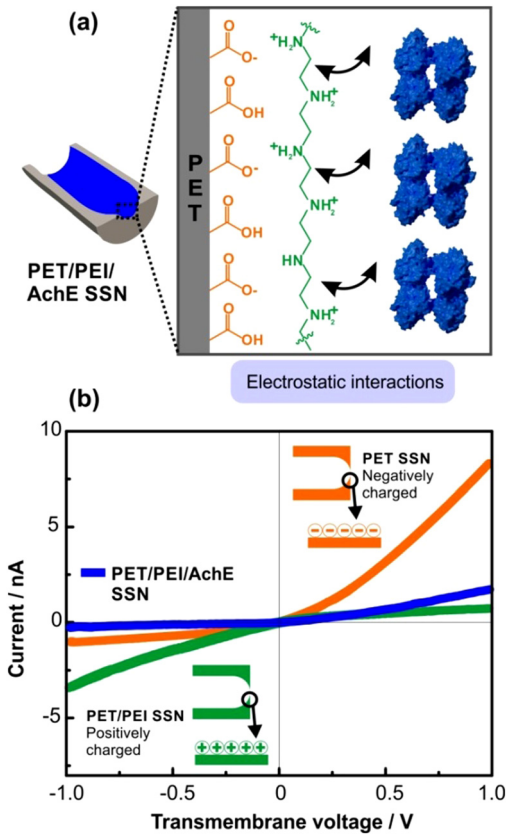

Fig. 1 (a) A scheme depicting the electrostatic interactions between PET carboxylate groups, PEI amino groups, and charged groups of AchE in the PET/PET/AchE SSN. (b) *I–V* curves for the different modification steps measured in 10 mM KCl at pH 7; bare PET nanochannel (orange), after the modification with PEI (green), and, finally, after AchE assembly (blue).

of the enzyme.[16] Thus, PET/PEI SSNs were exposed to a 1 mg mL^{-1} AchE solution at pH 7.4 (since the isoelectric point of AchE is 5.3,[17] the protein is negatively charged at this pH). One of the most important features of asymmetric nanochannels is that, depending on the sign and magnitude of their surface charges, they are able to rectify ionic currents passing through them.[18]

In addition, various factors such as the size of the nanochannel, the ionic strength, and the presence of specific ionic moieties determine the rectification behavior of the nanochannel.[19–22] Ion current rectification, *i.e.* the ion flux being favored at one polarity voltage compared with the opposite polarity, is a complex phenomenon caused by an electrical potential symmetry disruption that occurs in both charged asymmetric nanochannels (conical or bullet-shaped nanochannels) and asymmetrically functionalized nanochannels.[23–29] Fig. 1b displays the current–voltage (*I–V*) curves (experimental set-up in Fig. S2, ESI†) recorded at pH 7 before (PET SSN) and after the electrostatic self-assembly of PEI (PET/PEI SSN), and after the enzyme self-assembly (PET/PEI/AchE SSN). At pH 7, rectification takes place in a cation-selective regime (high conductance branch placed at positive transmembrane voltages, V_t), consistently with a negatively charged surface of the nanochannel provided by the carboxylate groups of PET. On the contrary, after PEI self-assembly, the device displays a clear rectification inversion, meaning that the ionic transport turns to the anion-selective rectifying regime (high conductance branch placed at negative V_t). This behavior is attributed to the surface charge reversion promoted by polyelectrolyte immobilization; at pH 7, most of the amino groups of PEI (pK_a 8–9) are protonated (positively charged), whereas PET carboxylic acid groups remain negatively charged.[30] Electrostatic self-assembly is known to produce charge reversion by overcompensation of the initially negative charge.[15] Then, the anchoring of AchE is evidenced in the SSN response as a decrease in the current, which might be related to the reduction of the SSN cross-section due to the presence of the enzyme. Also, a new reversion (to the cation-selective regime) and a decrease of the rectification are observed, meaning that the amount of charges exposed by AchE is high enough to overcompensate the PEI/PET charges.[11] Moreover, an estimation of the amount of immobilized AchE on the PET/PEI surface was performed by SPR (Fig. S3, ESI†), resulting in a mass surface coverage of 570 ± 90 ng cm^{-2}, in line with previous reports on g-FETs.[31]

Besides, we studied the response of the PET/PEI and PET/PEI/AchE SSNs as a function of pH. The PET/PEI SSN showed a reversible response (ion current at −1 V) between pH 4 and 7, for at least 5 cycles (Fig. S4, ESI†), proving that local pH changes do not affect the integrity of the self-assembly on the SSN. The nanofluidic response of PET/PEI/AchE nanochannels is sensitive to pH, increasing the cation-driven rectification efficiency as the pH increases from 4 to 8 (Fig. S5, ESI†). The pH response allows the identification of an effective surface pK_a of 6.9 ± 0.1 for this functionalized SSN. Thus, at about pH 7, the gating response of the device is enhanced to a maximum extent. Also, the activity of cholinesterases (as AchE) is known to peak at around pH 7–8, falling off at acidic pH.[32] Thus, the initial working pH for all the experiments was settled at ∼7.

Subsequently, regarding Ach sensing, we explored the transduction mechanism of the device by measuring the *I–V* response and the rectification factor (f_{rec}, eqn (S2), ESI†) of PET/PEI and PET/PEI/AchE SSNs at different Ach concentrations. When exposing the PET/PEI/AchE SSNs to a 50 nM Ach solution (in 10 mM KCl, pH_0 = 7), a 26% change in f_{rec} (% Δf_{rec}) was observed (Fig. S6, ESI†). Moreover, an increment in the Ach concentration to 1 μM increased the observed change to 48%. On the contrary, upon the same process, the PET/PEI SSNs did not show a significant change in f_{rec} (0.4% for 1 μM Ach and not detectable for 50 nM Ach), meaning that the incorporation of AchE is necessary for the detection of Ach (Fig. S6, ESI†). As reported by Fenoy *et al.* for AchE-modified gFET-based biosensors, the AchE-catalyzed hydrolysis of Ach causes a decrease in the pH of the solution due to the generation of choline and acetic acid (AA).[31]

Similarly, Pérez-Mitta *et al.* showed that the catalysis of urea hydrolysis by urease-modified PET SSNs triggered an *I–V* response in accordance with the increase of the local pH of the device due to the production of ammonia.[11] Afterwards, it is clear that the Ach-dependent iontronic response of the PET/PEI/AchE SSN-based biosensors is generated by the confined enzymatic reaction that produces a change in the local pH

due to the release of AA (Fig. S6b, ESI†). Besides, we studied the pH-responsiveness of AchE to Ach in solution (Fig. S7, ESI†). The hydrolysis of Ach implies a pH decrease from 7 to 4 when using 1 mM Ach. These results validate the initial hypothesis that the transduction mechanism of the device relies on a local pH change stemming from the enzymatic reaction. We also studied the time response of the PET/PET/AchE SSN to Ach (Fig. S8, ESI†). The *I–V* response and f_{rec} stabilize after 30 min of treatment with a 100 μM Ach solution. With this kinetic experiment, a 30 min exposure time of the membranes in the presence of the analyte before the ionic transport measurements was established. Furthermore, the PET/PEI/AchE SSN Ach-dependent behavior was explored by using aqueous Ach solutions with concentrations ranging from 1 nM to 100 μM. Fig. 2a shows the *I–V* curves for the different substrate concentrations. As previously mentioned, at pH 7 the nanochannels are negatively charged due to the presence of AChE anchored to the surface. Then, the initial *I–V* curve in the absence of Ach displays a high conductance branch at V_t = 1 V (cation-driven rectification). However, exposing the membrane to Ach solutions, even in the nanomolar range, results in both a decline in the current at V_t = 1 V (high conductance branch) and an increase in the current at V_t = −1 V (low conductance branch). When the Ach concentration reaches a value of 50 μM, a clear inversion in the rectification direction can be seen and the current at V_t = −1 V becomes higher in module than the current at V_t = 1 V (Fig. 2a). These Ach-induced changes in the iontronic response can be analyzed in terms of f_{rec} as a function of the Ach concentration (Fig. 2b). At first (0 μM Ach, pH 7), f_{rec} is negative due to the net negative charge of the channel. Increasing the Ach concentration leads to the production of AA, a weak carboxylic acid that hydrolyses in water producing H^+, which causes a decrease in pH and the concomitant increase in the protonation degree of acid–base surface groups (Fig. S6b, ESI†). Thus, increasing the Ach concentration leads to the protonation of PET-COO^- to give PET-COOH and this diminishes the surface negative charge of the PET/PEI/AchE SSN. Although the reported PEI pK_a is around 8–9, a fraction of amine groups from PEI could remain unprotonated at pH 7 due to the pK_a distribution usually observed when studying adsorbed polyelectrolytes. Consequently, from 1 nM to 25 μM of Ach, f_{rec} slowly decreases in module in accordance with the protonation of PET-COO^- or remaining amine groups from PEI. Within this concentration range, the effect of pH on the surface charge density of the nanochannels is moderate as they are in the so-called isoelectric region.[15] However, the variation of the surface charge is high enough to be reliably and reproducibly detected by the iontronic response. More importantly, this device shows a well-defined linear relationship between f_{rec} and log([Ach]) in the nM range (Fig. 2c). As Fig. 2b shows, when the Ach concentration surpasses 25 μM, f_{rec} becomes positive, revealing that the isoelectric region is surpassed and the surface is positively charged. At this point of the calibration curve, most of the PET-COO^- groups are in their protonated form, and the surface charge is dominated by the positively charged PEI amine groups. The production of AA by the enzymatic reaction yields a stronger increment of the surface charge density leading to a higher sensitivity in terms of the rectification factor. Again, a linear dependence between f_{rec} and log[Ach] in the μM range (25–100 μM) is observed with an anion-selective behavior. Thus, our PET/PEI/AchE SSN can work in two different regimes—the nM range (1–2500 nM) and the μM range (25–100 μM)—with linear responses for Ach concentration decades and good sensitivities, which makes it a unique and versatile Ach SSN-based biosensor. Additionally, the limit of detection (LoD) of the Ach biosensor was calculated to be 3 times the standard deviation for the blank (10 mM KCl, pH 7), yielding a value of 16 nM. As reported by Kirsch *et al.*, the physiological concentrations of Ach are in the nM range.[6] In principle, this LoD would allow the detection of the neurotransmitter in the cerebrospinal fluid of persons with Alzheimer's disease and vascular dementia.[33] Of course, other issues arise when dealing with complex real samples, which could affect the response of the present device; however, this illustrates the potentiality of the strategy. Regarding SSN-based sensors, until now there has been only one study that reports the construction of a biomimetic nanochannel by self-assembly of PEI and *p*-sulfonatocalix[4]-arene as the Ach recognition element (host–guest interaction mechanism).[34] Even though

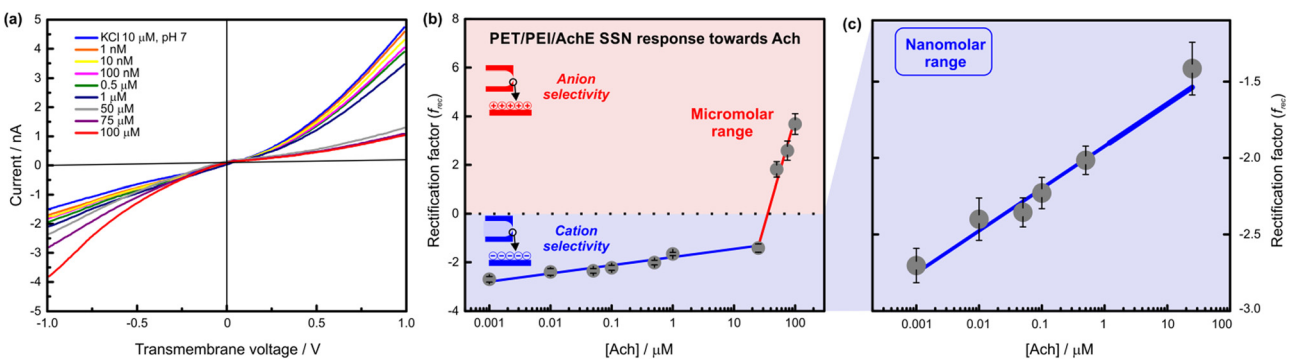

Fig. 2 (a) *I–V* curves recorded at different Ach concentrations, from 0 to 100 μM, in 10 mM KCl at pH 7. Every measurement was carried out *in situ* after a 30-minute exposure time. (b) Changes in f_{rec} for different Ach concentrations. (c) The PET/PEI/AchE calibration curve in the nanomolar region. Linear regressions for the nanomolar (1–2500 nM) and the micromolar range (25–100 μM) were made, in both cases resulting in $R^2 > 0.95$.

this device shows responsivity towards Ach in the nM range, the dependence between [Ach] and I (+2 V) is not linear.[34] However, there are several reported sensors based on other technologies.[31,35,38] For the sake of comparison, Table S1 (ESI†) shows the detection range and the LoD of the present biosensor and other recently reported enzymatic nanosensors for Ach detection. When compared with devices involving the immobilization of AchE on graphene FETs, this SSN device showed a significantly lower LoD (Table S1, ESI†).

As previously mentioned, the AchE activity is known to fall off at acidic pH, which can negatively impact the biosensor performance.[31,32] To address this point, we investigated the reversibility (and reusability) of the biosensor when alternating exposures to a blank solution (10 mM KCl, pH 7) and a 100 μM Ach solution (10 mM KCl, pH 7) (Fig. S9, ESI†). In particular, we used the higher Ach concentration that gave a linear response between f_{rec} and log([Ach]) (Fig. 2b), which is equivalent to 1/10 of the substrate inhibition concentration ($\sim$1 mM).[36] After carrying out 4 repetitive cycles, the biosensors did not lose their responsive behavior (Fig. S9, ESI†). Last but not least, the selectivity of the device response towards Ach was studied in comparison with other potential interferences that might be present in brain extracellular fluid: serotonin (SA), dopamine (DA), glucose (Glc), L-cysteine (L-cys), and ascorbic acid (AA). The concentrations tested were chosen based on their corresponding levels found in the brain extracellular fluid.[5,37] The change in f_{rec} (% Δf_{rec}) is significantly lower when exposing the membrane to 10 μM SA, 1 mM Glc, 50 μM DA, 10 μM L-cys, or 200 μM AA compared with the change provoked by the subsequent exposure to 50 μM Ach (Fig. S10, ESI†). Thus, the selectivity of the iontronic response towards Ach must be ascribed to the AchE enzyme specificity for the recognition of Ach over other molecules.[9]

In conclusion, we have rationally designed and created an Ach-responsive biosensor based on the integration of the enzyme AchE in single nanochannels functionalized with PEI. The working principle of this sensor relies on the strong dependence of the ionic transport properties of nanofluidic diodes on the nature of their surface charges. The weak polyelectrolyte acts as a ''chemical amplifier'' of the enzymatic process as it increases the sensitivity of the detection of local pH changes. Importantly, these nanofluidic sensors were able to operate reliably and reproducibly in the nanomolar range, yielding a 16 nM LoD. Also, the biosensors displayed a remarkably reversible and selective response towards Ach. To the best of our knowledge, this is the first report of an enzymatic nanofluidic Ach biosensor and, as such, we believe that further elaboration of this sensing strategy will open up new avenues for highly sensitive detection of different neurotransmitters.

Conflicts of interest

There are no conflicts to declare.

References

1 World Health Organization, Neurological Disorders: Public Health Challenges, World Health Organization Press, Geneva, Switzerland, 2007.
2 L. Gan, M. R. Cookson, L. Petrucelli and A. R. La Spada, *Nat. Neurosci.*, 2018, **21**, 1300–1309.
3 S. E. Hyman, *Curr. Biol.*, 2005, **15**, R154–R158.
4 M. Hasanzadeh, N. Shadjou and M. de la Guardia, *TrAC, Trends Anal. Chem.*, 2017, **86**, 107–121.
5 K. M. Mitchell, *Anal. Chem.*, 2004, **76**, 1098–1106.
6 S. H. Kirsch, W. Herrmann, Y. Rabagny and R. Obeid, *J. Chromatogr. B: Anal. Technol. Biomed. Life Sci.*, 2010, **878**, 3338–3344.
7 S. Andreescu and J.-L. Marty, *Biomol. Eng.*, 2006, **23**, 1–15.
8 R. Sangubotla and J. Kim, *TrAC, Trends Anal. Chem.*, 2018, **105**, 240–250.
9 G. Laucirica, Y. T. Terrones, V. Cayón, M. L. Cortez, M. E. Toimil-Molares, C. Trautmann, W. Marmisollé and O. Azzaroni, *TrAC, Trends Anal. Chem.*, 2021, **144**, 116425.
10 G. Pérez-Mitta, M. E. Toimil-Molares, C. Trautmann, W. A. Marmisollé and O. Azzaroni, *Adv. Mater.*, 2019, **31**, 1901483.
11 G. Pérez-Mitta, A. S. Peinetti, M. L. Cortez, M. E. Toimil-Molares, C. Trautmann and O. Azzaroni, *Nano Lett.*, 2018, **18**, 3303–3310.
12 R. Spohr, *Ion Tracks and Microtechnology: Principles and Applications*, Vieweg + Teubner Verlag, 1st edn, 1990.
13 P. Y. Apel, I. V. Blonskaya, S. N. Dmitriev, O. L. Orelovitch, A. Presz and B. A. Sartowska, *Nanotechnology*, 2007, **18**, 305302.
14 M. Tagliazucchi and I. Szleifer, *Chemically Modified Nanopores and Nanochannels*, Elsevier Inc., 1st edn, 2016.
15 G. Pérez-Mitta, A. Albesa, F. M. Gilles, M. E. Toimil-Molares, C. Trautmann and O. Azzaroni, *J. Phys. Chem. C*, 2017, **121**, 9070–9076.
16 R. A. Sheldon and S. van Pelt, *Chem. Soc. Rev.*, 2013, **42**, 6223–6235.
17 W. Leuzinger, A. L. Baker and E. Cauvin, *Proc. Natl. Acad. Sci. U. S. A.*, 1968, **59**, 620–623.
18 C. Chad Harrell, Z. S. Siwy and C. R. Martin, *Small*, 2006, **2**, 194–198.
19 C. Wei, A. J. Bard and S. W. Feldberg, *Anal. Chem.*, 1997, **69**, 4627–4633.
20 Z. Siwy, E. Heins, C. C. Harrell, P. Kohli and C. R. Martin, *J. Am. Chem. Soc.*, 2004, **126**, 10850–10851.
21 G. Pérez-Mitta, A. G. Albesa, C. Trautmann, M. E. Toimil-Molares and O. Azzaroni, *Chem. Sci.*, 2017, **8**, 890–913.
22 G. Laucirica, G. Pérez-Mitta, M. E. Toimil-Molares, C. Trautmann, W. A. Marmisollé and O. Azzaroni, *J. Phys. Chem. C*, 2019, **123**, 28997–29007.
23 Z. S. Siwy, *Adv. Funct. Mater.*, 2006, **16**, 735–746.
24 P. Ramírez, P. Y. Apel, J. Cervera and S. Mafé, *Nanotechnology*, 2008, **19**, 315707.
25 G. Laucirica, W. A. Marmisollé, M. E. Toimil-Molares, C. Trautmann and O. Azzaroni, *ACS Appl. Mater. Interfaces*, 2019, **11**, 30001–30009.
26 W. Guo, Y. Tian and L. Jiang, *Acc. Chem. Res.*, 2013, **46**, 2834–2846.
27 X. Huang, X. Y. Kong, L. Wen and L. Jiang, *Adv. Funct. Mater.*, 2018, **28**, 1801079.
28 Z. S. Siwy and S. Howorka, *Chem. Soc. Rev.*, 2010, **39**, 1115–1132.
29 L. Yang, P. Liu, C. Zhu, Y. Zhao, M. Yuan, X.-Y. Kong, L. Wen and L. Jiang, *Chin. Chem. Lett.*, 2021, **32**, 822–825.
30 M. Ali, Q. H. Nguyen, R. Neumann and W. Ensinger, *Chem. Commun.*, 2010, **46**, 6690–6692.
31 G. E. Fenoy, W. A. Marmisollé, O. Azzaroni and W. Knoll, *Biosens. Bioelectron.*, 2020, **148**, 111796.
32 F. Bergmann, S. Rimon and R. Segal, *Biochem. J.*, 1958, **68**, 493–499.
33 J. Jia, J. Jia, W. Zhou, M. Xu, C. Chu, X. Yan and Y. Sun, *Chin. Med. J.*, 2004, **117**, 1161–1164.
34 L. Wen, Z. Sun, C. Han, B. Imene, D. Tian, H. Li and L. Jiang, *Chem. – Eur. J.*, 2013, **19**, 7686–7690.
35 M. P. S. Mousavi, M. K. Abd El-Rahman, A. M. Mahmoud, R. M. Abdelsalam and P. Bühlmann, *ACS Sens.*, 2018, **3**, 2581–2589.
36 I. B. Wilson and J. Alexander, *J. Biol. Chem.*, 1962, **237**, 1323–1326.
37 Y. Zhang, N. Jiang and A. K. Yetisen, *Biosens. Bioelectron.*, 2021, **189**, 113351.
38 M.-S. Chae, Y. K. Yoo, J. Kim, T. G. Kim and K. S. Hwang, *Sens. Actuators, B*, 2018, **272**, 448–458.